Published in Applied Optics 44, issue 28, 5928-5936, 2005
which should be used for any reference to this work

Confocal microscopy using variable-focal-length microlenses and an optical fiber bundle

Lisong Yang, Aaron Mac Raighne, Eithne M. McCabe, L. Andrea Dunbar, and Toralf Scharf

The use of variable-focal-length (VFL) microlenses can provide a way to axially scan the foci across a sample by electronic control. We demonstrate an approach to coupling VFL microlenses individually to a fiber bundle as a way to create a high-throughput aperture array with a controllable aperture pattern. It would potentially be applied in real-time confocal imaging *in vivo* for biological specimens. The VFL microlenses that we used consist of a liquid-crystal film sandwiched between a pair of conductive substrates for which one has a hole-patterned electrode. One obtains the variation of the focal length by changing the applied voltage. The fiber bundle has been characterized by coupling with both coherent and incoherent light sources. We further demonstrate the use of a VFL microlens array in combination with the fiber bundle to build up a confocal system. The axial response of the confocal system has been measured without mechanical movement of the sample or the objective, and the FWHM is estimated to be approximately 16 μm, with asymmetric sidelobes.

1. Introduction

Confocal optical microscopy has been widely used in biomedical science and material science for its unique sectioning property and its improved lateral resolution compared with the conventional alternative.[1] A traditional confocal microscope images a single point with high resolution by restricting the collected light from a sample to that reflected or emitted from the focal spot region of the objective lens. For this reason the field of view is narrow. To obtain an image of the sample, one needs a three-dimensional scan. One development of confocal microscopy involves techniques to achieve real-time imaging without compromising resolution. The use of a Nipkow disk as a pinhole array is the first approach to providing real-time quasi-confocal imaging with reduced scanning in the lateral direction.[2] However, the primary problem in using a Nipkow disk is its low light throughput (~4%), which is due to the large mark–space ratios of ~5 required for reducing the cross talk between neighboring pinholes in the disk without compromising the system's resolution.[3] A combination of a microlens array and a Nipkow disk offers an improvement in the light throughput of as much as 60% by matching the foci of the microlenses to the pitch and diameter of the pinholes.[4] Further development involves the design of a real-time clinical confocal endoscope; a confocal imaging system with a miniature objective and a flexible fiber bundle has been studied.[5] The fiber bundle can act as both a pinhole array and an image-carrying element. Normally an imaging fiber bundle has a mark–space ratio of 2 if it is used as a pinhole array. The cross talk between neighboring fibers will degrade the confocal images. Thus Juškaitis *et al.*[6] described a real-time confocal microscope that views a fiber bundle in parallel to a Nipkow disk at its proximal end. McCabe[7] proposed a system that for the first time applies a variable-focal-length (VFL) microlens array to selectively address a coherent fiber bundle and thus achieve confocality. Smith *et al.*[8] demonstrated switching of one VFL microlens into a single-mode fiber. These publications give us a hint that the cross talk between neighboring fibers can be suppressed by selective coupling of the light through the VFL microlenses into the individual fibers. In this paper, we investigate, for the first time to our knowledge, the possibility of achieving confocal imaging with the

L. Yang, A. Mac Raighne (macraiga@tcd.ie), E. M. McCabe, and L. A. Dunbar are with the Department of Physics, Trinity College Dublin, Dublin 2, Ireland. T. Scharf is with the Institute of Microtechnology, University of Neuchâtel, 2000 Neuchâtel, Switzerland. L. Yang is also with the Institute for Experimental Physics, Free University Berlin, 14195 Berlin, Germany, and L. A. Dunbar is also with the Institut de Photonique et d'Electronique Quantique, École Polytechnique Federal Lausanne, CH-1015 Lausanne, Switzerland.

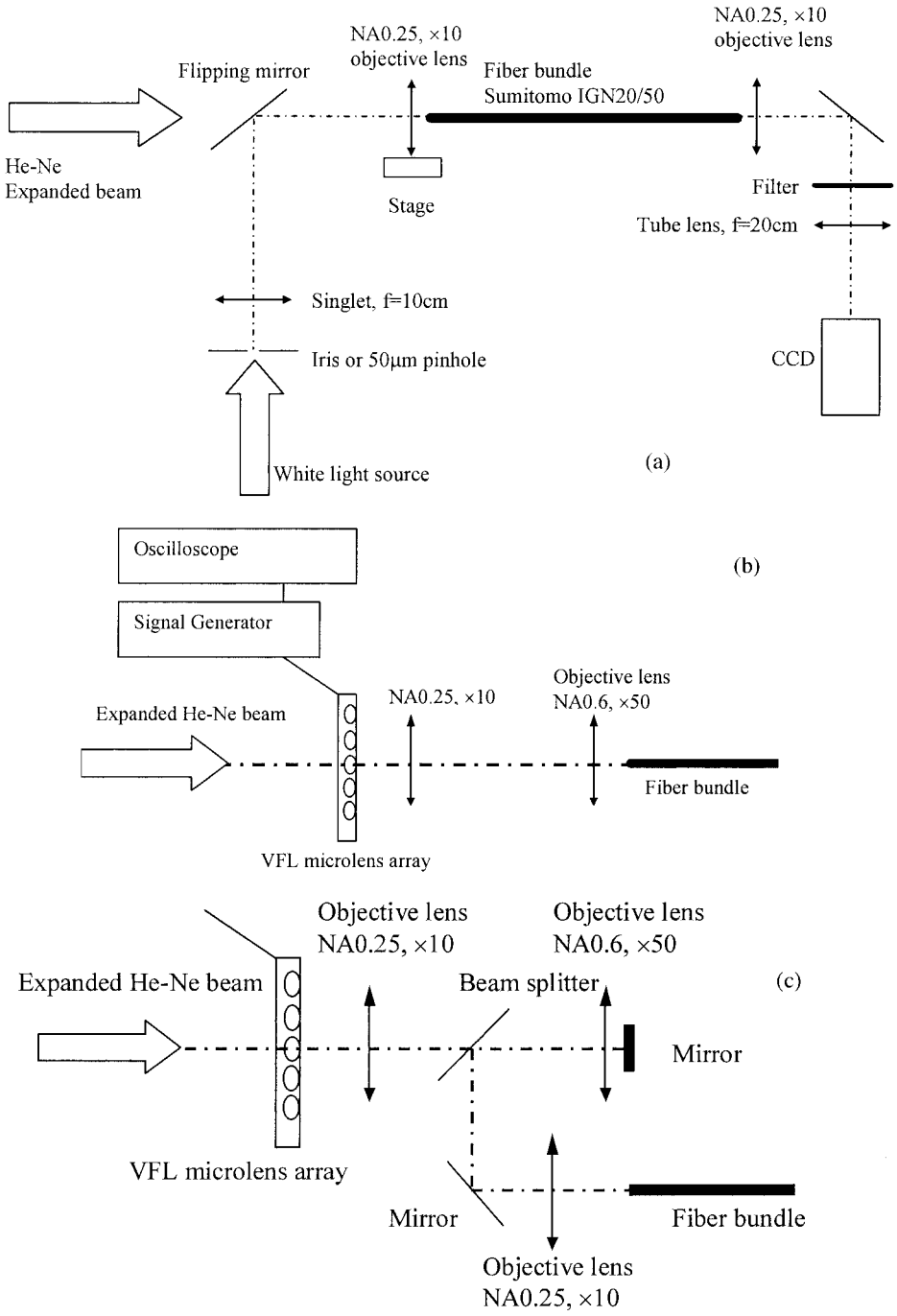

Fig. 1. Setups for (a) direct coupling of a fiber bundle with a He–Ne laser or a tungsten lamp, (b) a fiber bundle coupled with a microlens array, and (c) a confocal arrangement. The microlens array produces a point source array, and the fiber bundle works as a pinhole array.

combination of a VFL microlens array and an optical fiber bundle. First we demonstrate coupling between the VFL microlenses and the fiber bundle. Then we show that the use of VFL microlenses in the confocal system potentially permits optical sectioning by electronic scan across the sample. This sectioning avoids the inflexibility of the traditional mechanical scan, which involves movement of the lens or the sample. The approach can potentially be applied to a real-time confocal endoscope for *in vivo* studies.

2. Experimental Results and Discussions

A. Direct Fiber Bundle Coupling

We first studied the characteristics of the fiber bundle by directly coupling the light into the fiber bundle. The fiber bundle that we used is a Sumitomo IGN20/50 imaging bundle (2 m long) with 50,000 fibers; an individual fiber has a diameter of ~4 μm. The center-to-center spacing of two neighboring fibers is ~8 μm. The core diameter is ~2 mm. The

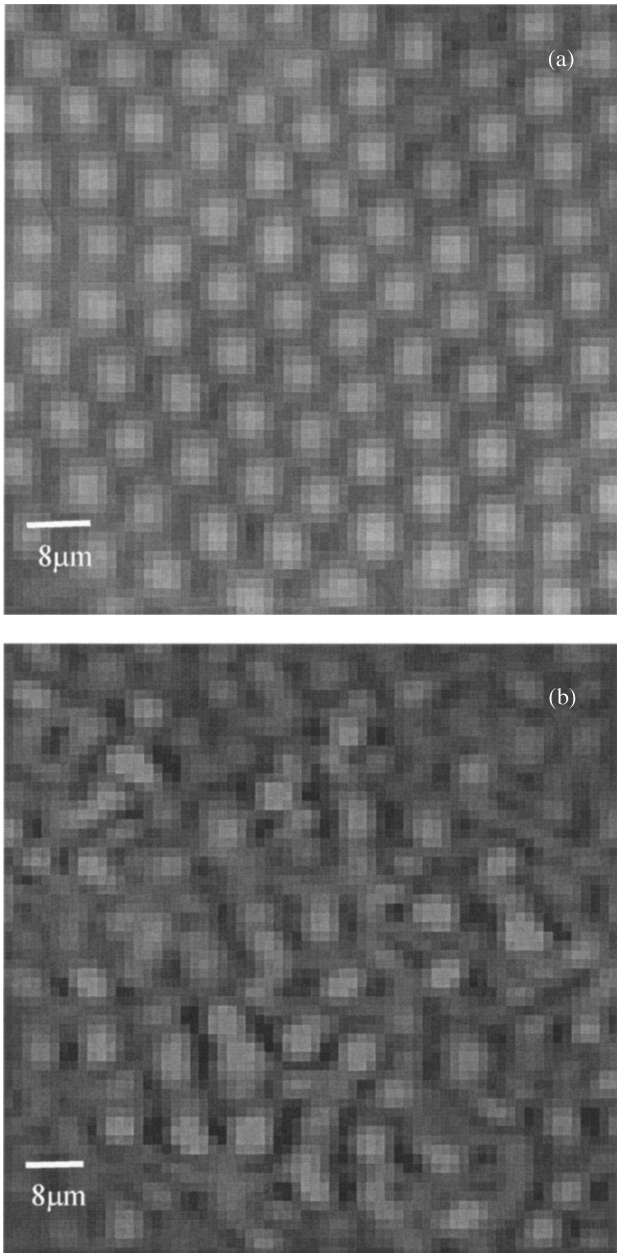

Fig. 2. Normalized images of the fiber bundle end when (a) tungsten incoherent light and (b) a He–Ne coherent laser source are used.

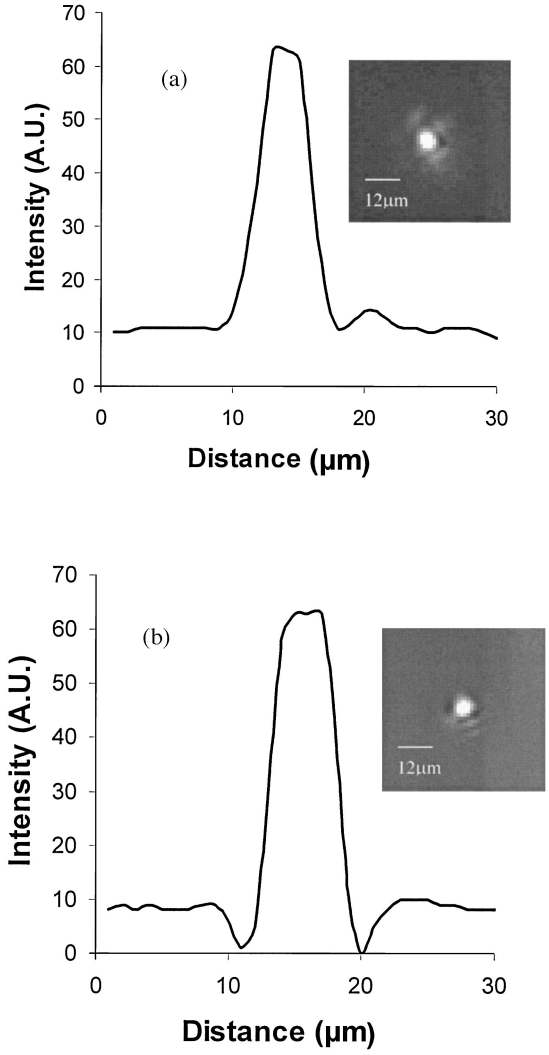

Fig. 3. Intensity profile of the single fiber inside the fiber bundle coupled with (a) a tungsten lamp and (b) a He–Ne laser. Insets, the corresponding images of the coupled fiber.

bundle was characterized by coupling with either a coherent and linearly polarized He–Ne laser (wavelength, 632.8 nm) source or incoherent and unpolarized tungsten white light by use of the setup shown in Fig. 1(a). The output power from the He–Ne laser is ~6 mW. For the white light, because it was not spatially well confined, an iris or a 50 μm pinhole was placed in the focus of a 10 cm focal-length lens as a spatial filter. The white light transmitted through the pinhole had a power of ~1 μW. The expanded He–Ne beam or collimated white light was coupled to the fiber bundle through a 10× objective lens. The effective numerical aperture (NA) of the objective was ~0.15. This objective lens was mounted onto a translational stage for focal movement in the Z direction. The fiber was mounted upon a two-dimensional stage for alignment of the fiber bundle in the XY directions. The two lenses after the bundle are the imaging lenses, which project a magnified image of the fiber bundle end onto the CCD camera. Neutral-density filters were used in the optical path of the He–Ne laser illumination to prevent saturation of the CCD cell.

When the face of the fiber bundle was placed off-focus for the objective lens, a large area of the fiber bundle was illuminated. Images of the fiber bundle end are shown in Fig. 2. When incoherent white light was used, the hexagonally packed fiber bundle could be clearly seen in the image, as shown in Fig. 2(a). However, for the coherent He–Ne laser source, the pattern of the fiber bundle was interrupted by the interference of the light emerging from neighboring fibers in the bundle, as shown in Fig. 2(b). The light throughput for a coherent light source is a few percent, depending on the position of

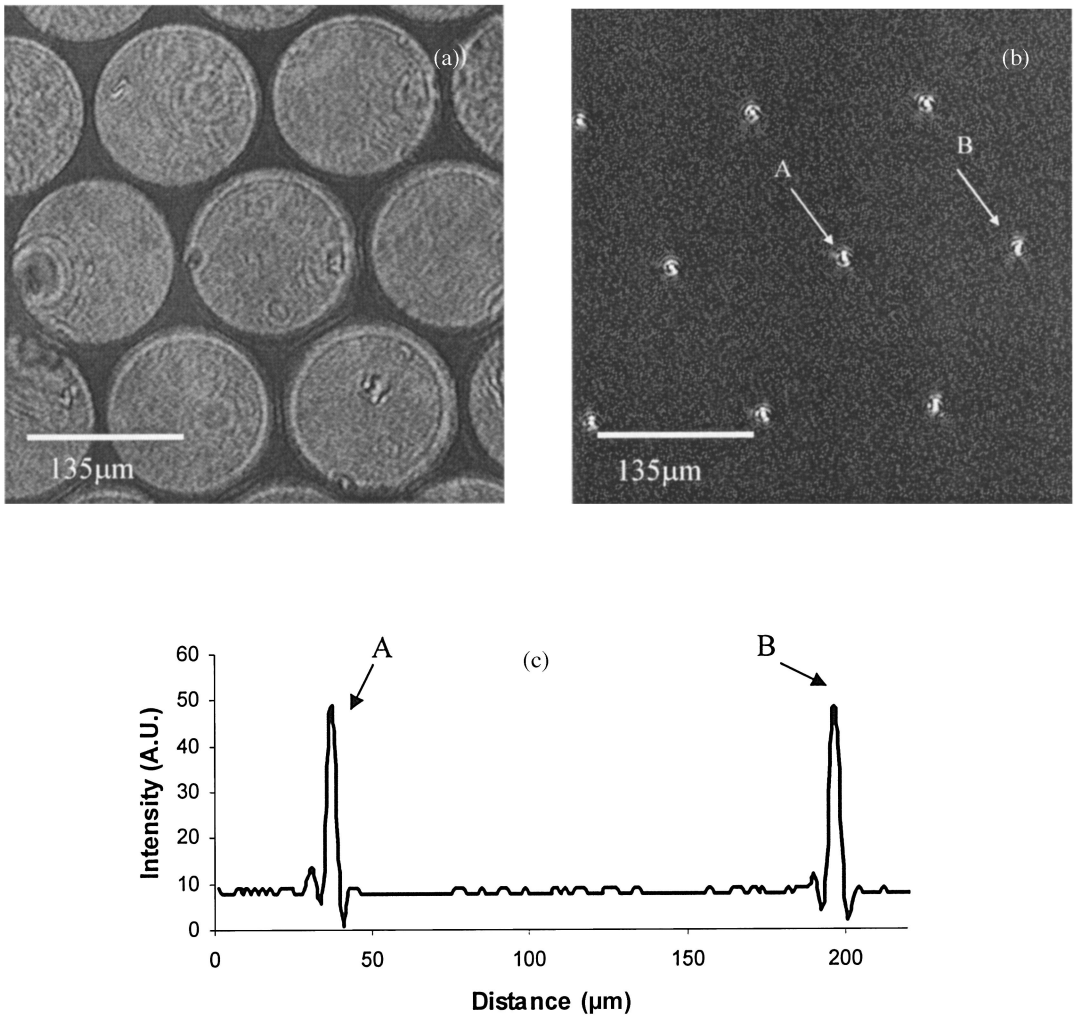

Fig. 4. Normalized image of (a) the VFL microlens array and (b) foci. (c) Profile of foci A and B in (b). The driving voltage (RMS) on the VFL microlenses is 2.83 V.

the fiber bundle. For incoherent light, the throughput is ~1%. When an individual fiber in the bundle is precisely aligned to the focus of the objective lens, the light can be well coupled into a single fiber. In the case of white light, a pinhole has to be used instead of an iris. The insets in Figs. 3(a) and 3(b) show the images of the coupled single fiber in the fiber bundle with a coupling efficiency (CE) of ~40% for a He–Ne laser and a CE of ~2% for a tungsten lamp. Figures 3(a) and 3(b) are the intensity profiles of the focal spots, correspondingly. The width of the profile measured by a Gaussian fit is ~4.0 μm, which agrees with the mode diameter of the fiber. The same intensity level has been subtracted from all the intensity profiles throughout this paper to account for noise. Note the nonzero background, which may be due to the leakage of light through the whole fiber bundle. In coherent light propagating along an individual fiber in a fiber bundle, there are always two minimal intensities below background, as shown in Fig. 3(b). This might be due to interference between neighboring fibers in which the scattered light that remains partly coherent plays an important role. The phenomenon does not appear in Fig. 3(a), for which incoherent light was used.

In what follows, we characterize a VFL microlens array and then utilize it as pointlike light sources to

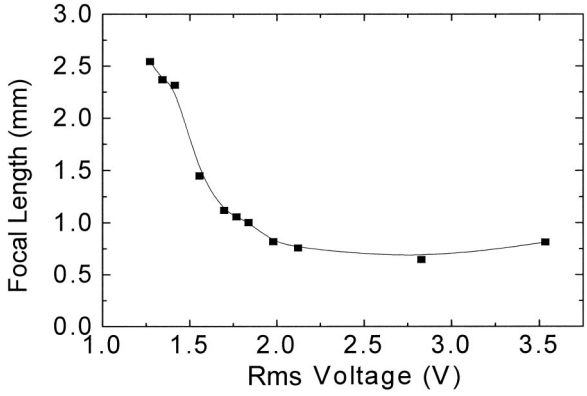

Fig. 5. Dependence of the focal length of the microlens on the applied voltage.

address selectively the individual fibers in a fiber bundle.

B. VFL Microlens Array

The VFL microlens can be obtained by use of liquid-crystal (LC) materials that show a large refractive-index anisotropy with a low driving voltage.[9,10] Our LC microlens has an asymmetric electrode structure of a hole-patterned electrode and a plane transparent electrode. Holes with diameters of 135 μm and center-to-center spacings of 155 μm were etched in the chromium electrode. The counterelectrode was made from transparent indium tin oxide. Both glass substrates were spin coated with alignment polymer and rubbed to give strong anchoring. With the two substrates, an antiparallel planar aligned LC cell was assembled with a thickness of 50 μm.[11] When voltage was applied, owing to the edge effects of patterned electrodes the electric field dropped off toward the center of the holes, which caused the LC to form a graded-index converging lens.[12]

The image obtained by our microscopic setup of the VFL microlenses with a hexagonal arrangement is shown in Fig. 4(a). The collimated He–Ne laser was used as a coherent and linearly polarized light source. The area covered by the lenses is more than 70% of the total cell. Consider the light lost by surface reflection from the substrate and by scattering of light in the LC cell; the lenses still can capture more than 50% of the light and focus it onto the virtual array of pinholes. Figure 4(b) shows images of foci with a driving root-mean-square (RMS) voltage of 2.83 V. The applied field has a sinusoidal wave with a frequency of 1 kHz from the signal generator. The intensity profile of two neighboring focal spots is plotted in Fig. 4(c). The full width at half-maximum (FWHM) of the focus is ~3.5 μm, which gives a NA of the microlenses of ~0.1. From Fig. 4(c) we can see the minimum intensities below the background that surrounds the focal spots. They might be due to interference of the scattered light from the VFL microlenses, which remains partly coherent. We could not obtain images of microlenses and their foci by using our incoherent light source because of the low intensity of the collimated white-light illumination on the microlens array.

By changing the applied voltage we could measure the variation of the focal length of the microlens, as shown in Fig. 5. The focal length ranges from 2542.5 μm (at 1.27 V) to 645 μm (at 2.83 V), where accordingly the NA ranges from 0.003 to 0.1. Note that, for the RMS voltage below 1.27 V, the electric field has not formed a lens shape and that, for the voltage above 2.1 V, only a slight change of the focal length can be observed. For voltages above 3 V, disinclinations appear and the lens properties are destroyed. Hence, in what follows, we focus our study mainly on the range 1.4–2.1 V, where the focal length of the microlenses varies sensitively with changes in voltage.

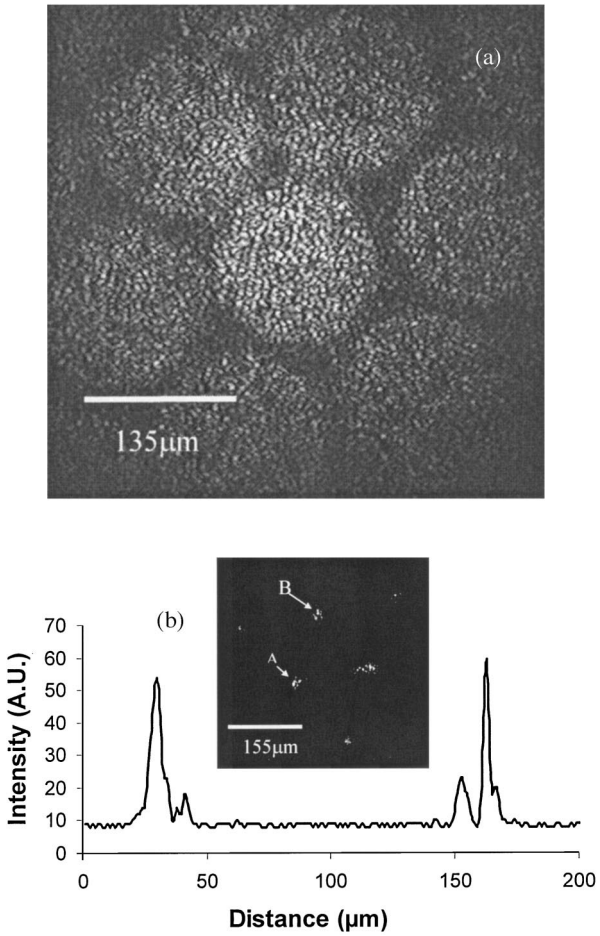

Fig. 6. (a) Normalized image of the microlens array transferred by the fiber bundle. (b) Intensity profile of two focal spots, A and B. The applied voltage is 1.77 V.

C. Fiber Bundle Coupling by VFL Microlenses

By using the setup shown in Fig. 1(b), we coupled the light into the fiber bundle through the microlenses. Because of the low power of our white light, only a He–Ne laser was selected as a light source. We cannot directly couple the light from microlenses into a fiber bundle because the focal plane of the microlenses is inside the cell when a maximum lens NA of 0.1 is used. Thus two objective lenses, 10×(NA, 0.25) and 50 × (NA, 0.65), were used between the microlenses and the fiber bundle. The lens system produces a maximum demagnification of 5×. By careful alignment of the distances between microlenses, objective lenses, and the fiber bundle, microlenses can be imaged onto the face of the bundle and then transferred to a CCD camera with different sets of demagnification. Figure 6(a) shows an image of the microlenses through the fiber bundle with a demagnification of ~1. When an electric field is applied, the microlenses focus the light. Adjusting the distance between the microlens and 10× objective in front, we can image the array of the foci onto the face of the fiber bundle, as shown in the inset of Fig. 6(b), for which the voltage was 1.77 V. As the focal spot of a single microlens approximates the mode diameter of an individual fiber, as we showed

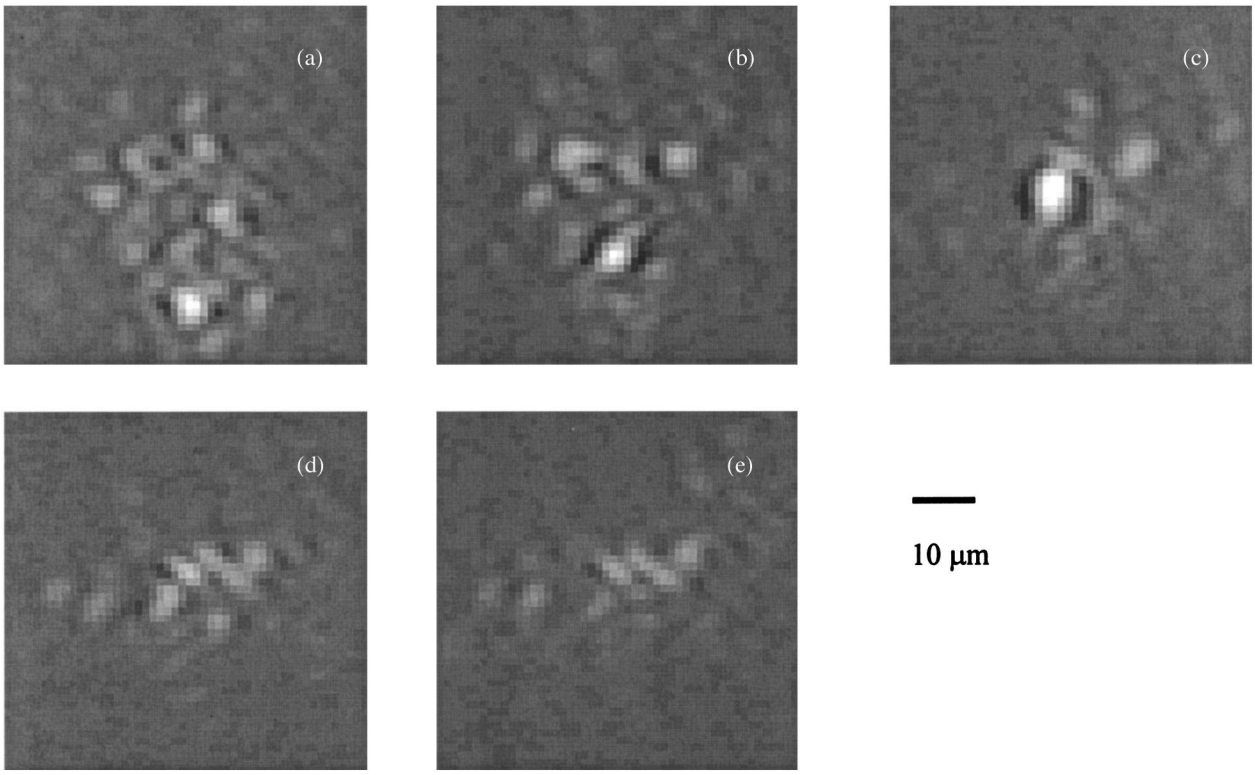

Fig. 7. Images of focal spot A as shown in the inset of Fig. 6(b). The applied voltages are (a) 1.41, (b) 1.56, (c) 1.77, (d) 1.98, and (e) 2.26 V.

in Figs. 3 and 4, good coupling between a microlens focus and a fiber tip can be obtained by careful alignment. The intensity profile in Fig. 6(b) shows two selected spots, A and B, of the coupled fibers with optimized coupling. Note that the interference minimum intensities through the microlens array, shown in Fig. 4(c), were reasonably well suppressed or canceled by the fiber bundle during light coupling. The distance between neighboring coupled fibers is ~160 μm. Hence there are ~20 idle fibers between 2 coupled fibers. The small number of splits shown in Fig. 6(b) is due to the fact that the fiber bundle does not have precisely the same hexagonally packed structure as the VFL microlens array has. Thus the mismatch between microlens focus and fiber tip is inevitable and gives an average CE of ~1% in our case. However, by developments in fabrication of the fiber bundle and the VFL microlens and by good design of the coupling optics, the CE may reach 40% of that of the typical lens-to-fiber coupling.

When we vary the applied voltage, the focal length of the microlenses changes. As a result, the focal array on the face of the fiber bundle will move along the optical axis. Figures 7(a), 7(b), 7(c), 7(d), and 7(e) show zoom-in images of focal spot A from Fig. 6 at different applied voltages, i.e., at 1.41, 1.56, 1.77, 1.98, and 2.26 V, respectively. For a voltage of 1.77 V, light was well coupled into individual fibers, as shown in both Fig. 6(b) and Fig. 7(c). In other cases, the fiber bundle was defocused and the light was split into several fibers. We take the average intensity over an area of 11 μm × 11 μm in the image of the fiber bundle end, where the well-coupled fiber is centered, and assume that the neighboring fibers beyond the selected area are invisible. The intensity responses of spots A and B shown in Fig. 6 are shown in Fig. 8 as a function of the applied voltage. The FWHM of the voltage response is ~0.5 V. For a system demagnification of ~1, this response width corresponds to a focal-length variation of ~750 μm in front of the fiber bundle according to the data shown in Fig. 5. The data analysis above shows that microlenses can address the individual fi-

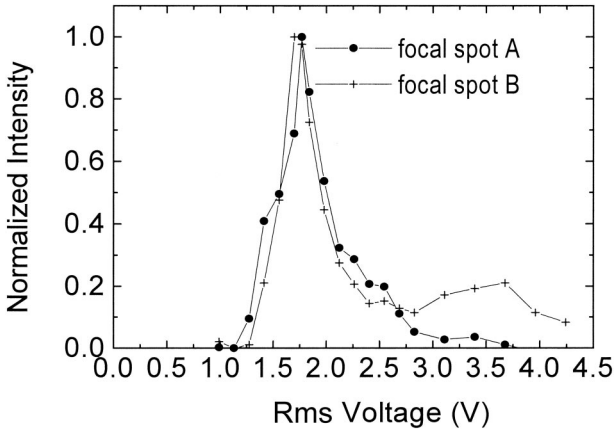

Fig. 8. Normalized intensity of focal spots A and B as shown in the inset of Fig. 6(b) versus supplied average. The intensity was averaged over an area of 11 μm × 11 μm.

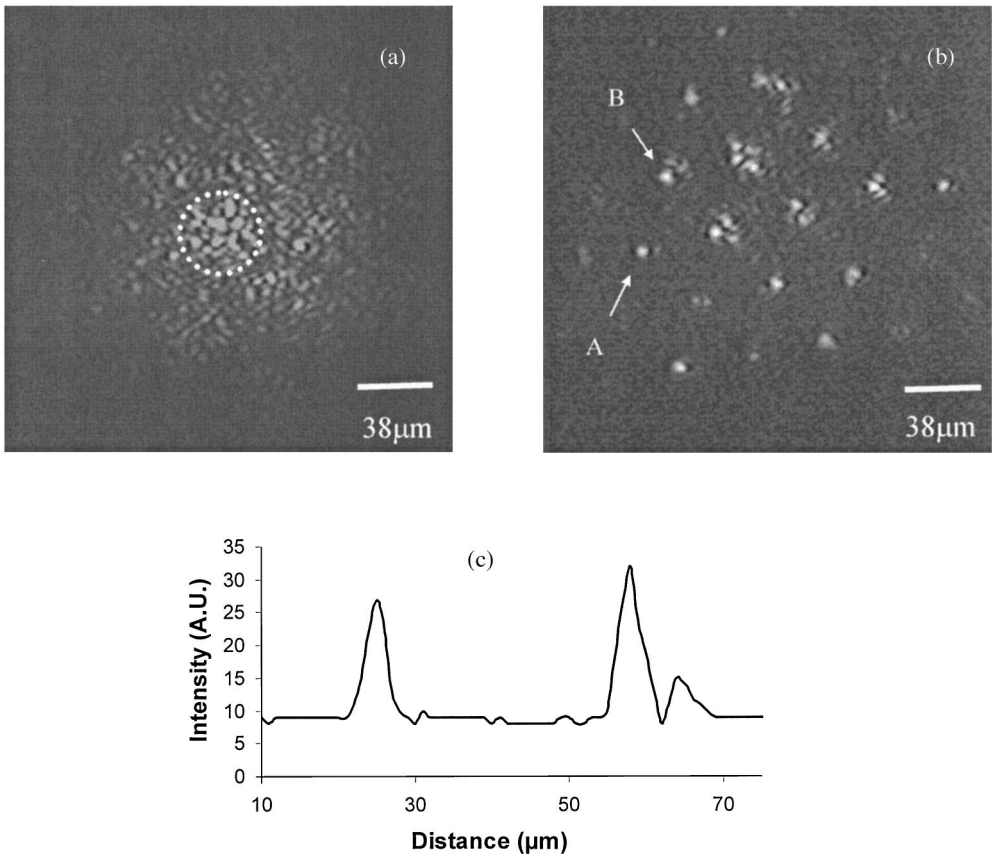

Fig. 9. (a) Normalized image of a microlens array guided by a fiber bundle. The dotted circle corresponds to a microlens. (b) Normalized image of the focal spots with 1.77 V voltage supplied. (c) Intensity profile of the two spots, A and B, as shown in (b).

bers and switch the fibers on and off electronically. They can potentially be applied in a real-time confocal endoscope for which the fiber bundle acts as a pinhole array.

Comparing the images in Fig. 7, we note that the overall light throughput from a well-coupled fiber bundle with a voltage of 1.77 V applied to VFL microlenses is only 1.5–3 times as much as that from a less-well-coupled fiber bundle under voltages from 1.4 to 2.26 V. This implies that our CE of one-to-one microlens–fiber coupling is rather low where the fiber bundle acts nearly as an image carrier. Besides, the interference between neighboring fibers that causes the speckle effect is believed to play a role as well. However, with the improvement in CE for microlens–fiber coupling and good control of fiber spacing in the bundle, we can expect to switch the individual fibers in the fiber bundle on and off by using VFL microlenses with a better signal-to-noise ratio so they can be used in a real-time confocal system.

When the microlens is moved close to the focal plane of the 10× objective lens and the fiber bundle close to the 50× objective lens, a larger demagnification can be obtained. Figure 9(a) shows images of microlenses with a system demagnification of ~4.2. Because of the interference of the coherent light emitted from the individual fibers in the bundle, the microlenses cannot be clearly distinguished. The dotted circle illustrates an ideal imaged microlens. However, when voltage is applied, the foci of the microlenses can be well coupled to the fiber bundle, as shown in Fig. 9(b). The intensity profile in Fig. 9(c) gives a coupled fiber spacing of ~37 μm, which means that there are ~4 idle fibers between the coupled neighbors. Although interference appears in this case and gives a worse signal-to-noise ratio than that in Fig. 6(b), the coupled foci still can be distinguished with

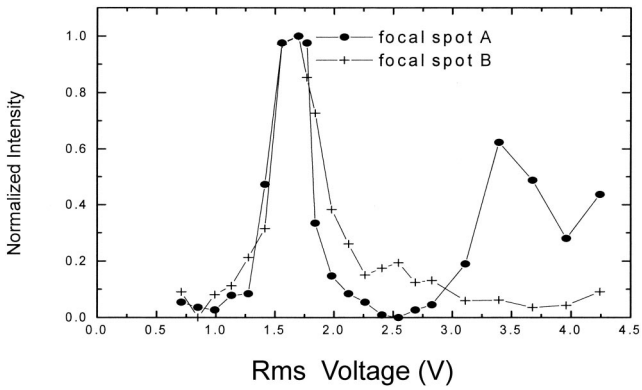

Fig. 10. Normalized intensity of the spots shown in Fig. 9(b) versus supplied average. The intensity is averaged over an area of 11 μm × 11 μm.

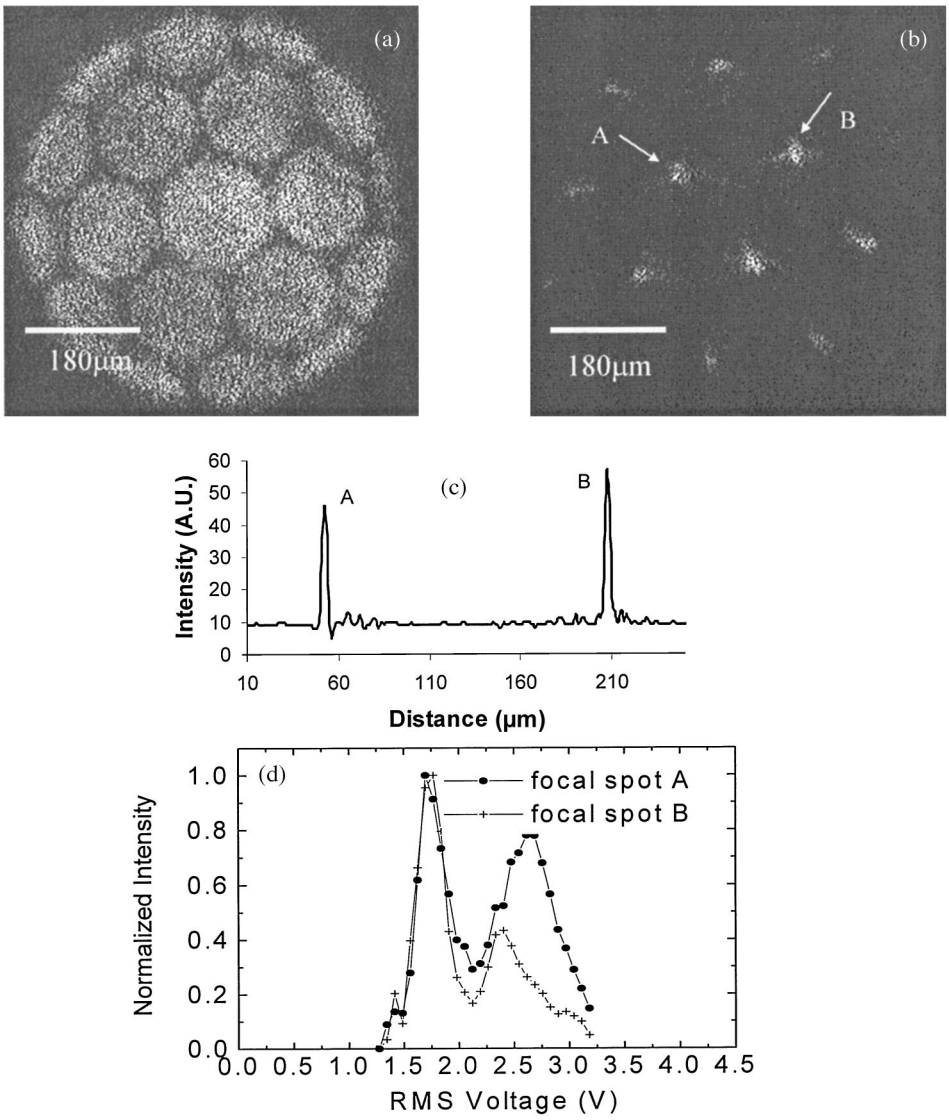

Fig. 11. (a) Normalized image of microlenses for the setup shown in Fig. 1(c). (b) Image of the focal spots with applied voltage 1.77 V. (c) Intensity profile of the two focal spots, A and B. (d) Normalized intensity of the focal spots versus supplied average. The intensity is averaged over an area of 11 μm × 11 μm that surrounds spot A or B, as shown in (b).

reasonable uniformity. This result suggests that, when the ratio between the coupled fiber spacing and the fiber diameter is ~5 or larger, the cross talk between fibers does not degrade the image much. Similarly, we measured the intensity response as a function of the applied voltage in the case of system demagnification of ~4.2, shown in Fig. 10. The FWHM of the voltage is ~0.5 V, which corresponds to a focal-length variation of ~750 μm/4.2^2 (≈43 μm) in front of the fiber bundle, according to geometrical optics. We attribute the extraordinary response behavior of spot A above 3.2 V to the possibility of deformation of the lens: When high voltage is applied, the focusing properties of the LC becomes irregular.

D. Confocal System with VFL Microlenses and Fiber Bundle

We further demonstrate that the combination of VFL microlens and fiber bundle is confocal. The setup is shown in Fig. 1(c); the microlens array produces a point source array, and the fiber bundle works as a pinhole array. We placed a mirror sample in the focal plane of the 50× objective lens. The light reflected from the mirror was coupled to the fiber bundle through a beam splitter and a 10× objective lens. The images of the microlens and the array of foci coupled to the fiber bundle at 1.77 V are shown in Figs. 11(a) and 11(b), respectively. The intensity profile gives us an image of lens spacing of ~176 μm; this indicates that the system is quasi-symmetric and has an overall magnification of ~1.13.

Applying the voltage causes the focal length of the microlens to vary, and, correspondingly, the array of focus after the 50× objective lens will axially scan the mirror sample. Therefore the axial response for the system can be measured while the fiber bundle acts as a pinhole array to block the off-focus signal away from the on-focus information to produce the optical

sectioning. The intensity response was measured over the output of the fiber bundle end, shown in Fig. 11(d). The intensity is an average over an area of 11 μm × 11 μm that surrounds spot A or B with maximum intensity. The FWHM is ~0.25 V, which is less than that of direct microlens-fiber-bundle coupling because of the sectioning property of the reflected confocal system. According to the data shown in Fig. 5, the change of voltage from 1.60 to 1.85 V will give a focal-length change of the microlens of ~400 μm. The microlenses are demagnified by a factor of 5 to the mirror. Based on geometrical optics, focal spots of the 50× objective lens vary at a distance of ~400 μm/5^2 (≈16 μm). Hence the FWHM of the system's axial response can be estimated to be ~16 μm. The NA of the microlens is varied from 0.047 to 0.068 as the voltage changes from 1.60 to 1.85 V. Hence the effective NA of a 50× objective in front of the mirror sample will be 0.23 to 0.34. As is known, for an ideal confocal system with only a pinhole, while the pinhole is infinitely small the FWHM of the axial response can be estimated as ~$0.9\lambda/NA_{obj}^2$, i.e., <11 μm, with a wavelength of 0.633 μm and an effective NA of the objective of 0.23. However, in our case, because of the cross talk between neighboring fibers in the bundle, the axial response of the system is degraded. In Fig. 11(d) the asymmetric sidelobes can be clearly observed. The second peak appears near the voltage of 2.5 V applied to the VFL microlenses, which give an effective NA of the objective in front of the sample of ~0.5. This high NA might be the cause of spherical aberration[13] and of an asymmetric axial response in the confocal system; another possibility might come from the effect of the tube length on the axial response while our objective lens is not infinitely corrected. Further study of this phenomenon is needed. The difference between the two axial response curves of spots A and B indicates that microlens focusing properties vary from lens to lens. Besides, the offset of focal spots to the fiber end will also cause the axial responses to be different.

3. Conclusions

We have demonstrated coupling between a VFL microlens array and an optical fiber bundle. This can be a realistic way to create a high-throughput aperture array with a controllable pattern by electronic control of the VFL microlenses to switch the fibers on and off individually. It has potential application in real-time confocal endoscopes. Although our current coupling efficiency of microlens-to-fiber coupling is far from satisfactory, a fiber bundle designed to meet the specifications of the microlens array would allow each microlens to be well coupled to the fibers. Other improvements of the technique will involve increases of transmission and switching speed of the VFL microlenses, the ability to address individual VFL microlenses, and control of microlens sizes and NA.

Much more research is needed before this system can be used to image with the resolution expected in confocal microscopy. The work on the homogeneity of the focusing properties of the LC cells would minimize the amount of calibration that would be needed across the images.

We thank Enterprise Ireland for financial support, Trinity College for the Trinity Award given to Aaron Mac Raighne, and the Institute of Microtechnology for supplying the microlenses that were vital to this study.

References

1. T. Wilson and C. Sheppard, *Theory and Practice of Scanning Optical Microscopy* (Academic, 1984).
2. M. D. Egger and M. Petráň, "New reflected-light microscope for viewing unstained brain and ganglion cells," Science **157,** 305–307 (1967).
3. E. M. McCabe, D. T. Fewer, A. C. Ottewill, S. J. Hewlett, and J. Hegarty, "Direct-view microscopy: optical sectioning strength for finite sized, multiple-pinhole arrays," J. Microsc. **184,** 95–105 (1996).
4. T. Tanaami, Y. Sugiyama, and K. Mikuriya, "High speed confocal laser microscopy," Yokogawa Tech. Rep. **19,** 7–10 (Yokogawa, 9-32 Nakacho 2-chome, Musashino-shi, Tokyo, Japan, 1994).
5. A. F. Gmitro and D. Aziz, "Confocal microscopy through a fiber-optic imaging bundle," Opt. Lett. **18,** 565–567 (1993).
6. R. Juškaitis, T. Wilson, and T. F. Watson, "Real-time white light reflection confocal microscopy using a fibre-optic bundle," Scanning **19,** 15–19 (1997).
7. E. McCabe, "Optical imaging systems," Irish patent S99 0004 (4 April 2001).
8. P. J. Smith, C. M. Taylor, E. M. McCabe, D. R. Selviah, S. E. Day, and L. G. Commander, "Switchable fiber coupling using variable-focal-length microlenses," Rev. Sci. Instrum. **72,** 3132–3134 (2001).
9. D. W. Berreman, "Variable focus liquid crystal lens system," U.S. patent 4,190,330 (26 February, 1980).
10. S. Sato, "Liquid crystal lens-cell with variable focal length," Jpn. J. Appl. Phy. **18,** 1679–1684 (1979).
11. T. Scharf, P. Kipfer, M. Bouvier, and J. Grupp, "Diffraction limited liquid crystal microlenses with planar alignment," Jpn. J. Appl. Phys. **39,** 6629–6636 (2000).
12. S. Nose, S. Masuda, and S. Sato, "Optical properties of a liquid crystal microlens with a symmetric electrode structure," Jpn. J. Appl. Phys. **30,** L2110–2112 (1991).
13. C. J. R. Sheppard, M. Gu, K. Brain, and H. Zhou, "Influence of spherical aberration on axial imaging of confocal reflection microscopy," Appl. Opt. **33,** 616–624 (1994).